

Detection of Diffuse Hot Gas Around the Young, Potential Superstar Cluster H72.97–69.39

TRINITY L. WEBB,¹ JENNIFER A. RODRIGUEZ,¹

THESE AUTHORS CONTRIBUTED EQUALLY TO THIS WORK.

LAURA A. LOPEZ,^{1,2,3} ANNA L. ROSEN,^{4,5} LACHLAN LANCASTER,^{6,3,*} OMNARAYANI NAYAK,⁷ ANNA F. MCLEOD,^{8,9}
PAARMITA PANDEY,^{1,2} GRACE M. OLIVIER¹⁰

¹*Department of Astronomy, The Ohio State University, 140 W. 18th Ave., Columbus, OH 43210, USA*

²*Center for Cosmology and AstroParticle Physics, The Ohio State University, 191 W. Woodruff Ave., Columbus, OH 43210, USA*

³*Center for Computational Astrophysics, Flatiron Institute, 162 5th Avenue, New York, NY 10010, USA*

⁴*Department of Astronomy, San Diego State University, 5500 Campanile Dr, San Diego, CA 92182, USA*

⁵*Computational Science Research Center, San Diego State University, 5500 Campanile Dr, San Diego, CA 92182, USA*

⁶*Department of Astronomy, Columbia University, 550 W 120th St, New York, NY 10025, USA*

⁷*Space Telescope Science Institute, 3700 San Martin Drive, Baltimore, MD 21218, USA*

⁸*Centre for Extragalactic Astronomy, Department of Physics, Durham University, South Road, Durham DH1 3LE, UK*

⁹*Institute for Computational Cosmology, Department of Physics, University of Durham, South Road, Durham DH1 3LE, UK*

¹⁰*Department of Physics and Astronomy and George P. and Cynthia Woods Mitchell Institute for Fundamental Physics and Astronomy, Texas A&M Univeersity, 4242 TAMU, College Station, TX 77843-4242 USA*

ABSTRACT

We present the first Chandra X-ray observations of H72.97–69.39, a highly-embedded, potential super-star cluster (SSC) in its infancy located in the star-forming complex N79 of the Large Magellanic Cloud. We detect particularly hard, diffuse X-ray emission that is coincident with the young stellar object (YSO) clusters identified with JWST, and the hot gas fills cavities in the dense gas mapped by ALMA. The X-ray spectra are best fit with either a thermal plasma or power-law model, and assuming the former, we show that the X-ray luminosity of $L_X = (1.5 \pm 0.3) \times 10^{34}$ erg s⁻¹ is a factor of ~ 20 below the expectation for a fully-confined wind bubble. Our results suggest that stellar wind feedback produces diffuse hot gas in the earliest stages of massive star cluster formation and that wind energy can be lost quickly via either turbulent mixing followed by radiative cooling or by physical leakage.

Keywords: Young star clusters — HII regions — Stellar wind bubbles

1. INTRODUCTION

Massive stars are born in clustered environments (Krumholz et al. 2019), depositing substantial energy and momentum to the surrounding interstellar medium (ISM) through a variety of feedback mechanisms. In particular, fast, line-driven stellar winds (with velocities of $v_w \sim 10^3$ km s⁻¹) sweep up surrounding gas and create low-density cavities shock-heated to $\sim 10^7$ K temperatures (Castor et al. 1975; Weaver et al. 1977; Cantó et al. 2000; Stevens & Hartwell 2003; Harper-Clark & Murray 2009). Diffuse X-ray emission associated with these fast stellar winds has been detected from numerous massive star clusters (MSCs) in the Milky Way (Moffat et al. 2002; Yusef-Zadeh et al. 2002; Townsley et al. 2003;

Muno et al. 2006; Townsley et al. 2011) and the Magellanic Clouds (Townsley et al. 2006; Lopez et al. 2011, 2014). Although the integrated kinetic energy carried in the stellar winds is comparable to the kinetic energy delivered by supernova explosions (Agertz et al. 2013), the actual dynamical impact of the stellar wind feedback and how it evolves over time remains uncertain.

One open issue is the role of winds in the early evolution of MSCs, and the study of young, embedded sources can provide important insights. Toward this end, the highly embedded N79 star-forming complex in the southwestern region of the Large Magellanic Cloud (LMC; see Figure 1), which has an accelerating star-formation rate of ~ 2 times that of the starburst region 30 Doradus (hereafter 30 Dor; Ochsendorf et al. 2017), is an ideal target to study the role of stellar wind feedback at the onset of star cluster formation. The N79 region spans across ~ 500 pc and has three giant molecular cloud (GMC) complexes - N79 East, N79 West, and N79 South (see Figure 1; Wong et al. 2011;

Corresponding author: Trinity Webb
webb.916@osu.edu

* Simons Fellow

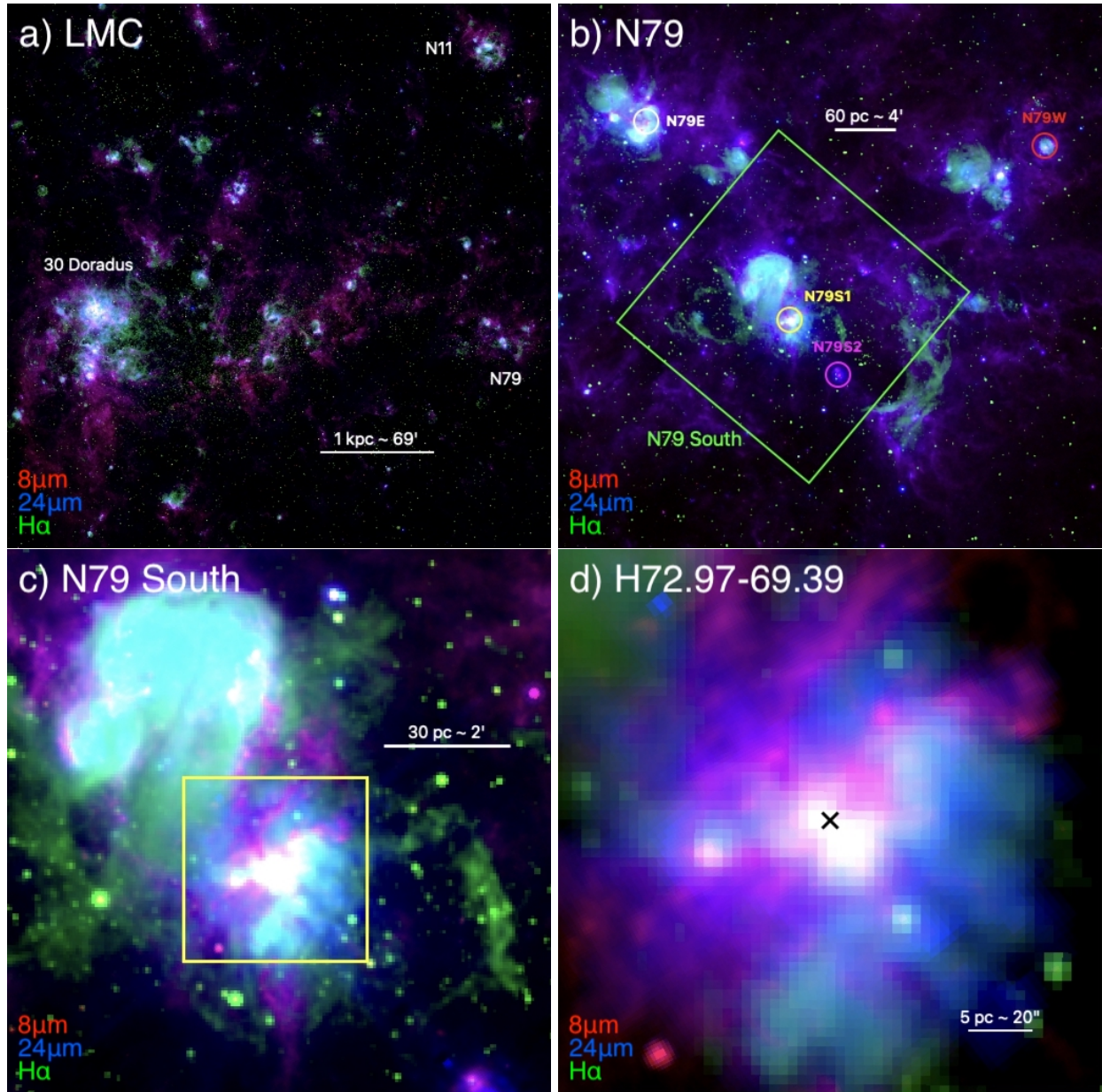


Figure 1. Three-color images, with Spitzer SAGE $8\mu\text{m}$ in red, Spitzer SAGE $24\mu\text{m}$ in blue (Meixner et al. 2006), and $\text{H}\alpha$ in green (Smith & MCELS Team 1998). North is up, East is left. (a) Large-scale, three-color image of the Large Magellanic Cloud. (b) Zoomed in three-color image of N79 showing the location of the three star-forming complexes: N79 East, N79 West, and N79 South. Two Spitzer-identified clusters of young stellar objects (YSOs) within N79 South are labeled N79S1 (the location of H72.97–69.39) and N79S2. The green box surrounding N79 South is the field of view of the Chandra ACIS-I observations. (c) Zoomed in three-color image of N79 South. The yellow box indicates the area surrounding H72.97–69.39 as shown in panel d. (d) Zoomed in three-color image the vicinity of H72.97–69.39 (black X).

Nayak et al. 2019). N79 South harbors a newly forming (<0.5 Myr old; Ochsendorf et al. 2017) potential proto-

superstar cluster (SSC) H72.97–69.39¹ based on its in-

¹This source is catalogued as HSOBMHERICC J72.971176–69.391112 (Seale et al. 2014, ; hereafter H72.97–69.39) and will be referred to as H72.97–69.39 throughout this paper. The position of H72.97–69.39 was refined by Nayak et al. (2019) based on the compact core’s continuum emission to R.A. 72.972201 and decl. –69.391301.

ferred bolometric luminosity ($\sim 2 \times 10^6 L_\odot$) and accelerating star-formation rate (Seale et al. 2014; Ochsendorf et al. 2017; Nayak et al. 2019). In comparison, R136 (the star cluster powering 30 Dor) has a luminosity of $\sim 7.8 \times 10^7 L_\odot$ (Malumuth & Heap 1994) and a decelerating star-formation rate. Both 30 Dor and N79 are on opposite leading edges of the LMC’s spiral arms (Ochsendorf et al. 2017), possibly facilitating their starburst activity due to large-scale dynamical inflows along the tidal tails. While R136 is 2 Myr old (Hunter et al. 1995), H72.97–69.39 is in the earliest stages of formation, offering an interesting point of comparison.

Previous studies of H72.97–69.39 have mapped the N79 star-forming complex in optical, infrared, and sub-mm wavelengths (Ochsendorf et al. 2017; Nayak et al. 2019, 2023), tracing the young stars, the cold molecular gas, and the dust. Here we study the X-ray emission of H72.97–69.39 with the Chandra X-ray Observatory, and we explore stellar-wind feedback at an early stage ($\lesssim 0.5$ Myr) in star formation. Specifically, we show the spatial distribution of the hot gas relative to the other gas phases, dust, and stars as well as compare the X-ray luminosity and hot-gas temperature predictions from wind bubble models. For comparison, the sample of 32 HII regions (including the full N79-South complex) examined by Lopez et al. (2014) had estimated ages of 3 – 10 Myr, when the sources’ shells had expanded ~ 4 – 150 pc. The other SSC in the LMC, R136 in 30 Dor, has been observed extensively by Chandra, including an X-ray Visionary Project (PI: L. Townsley) totaling ~ 2 Ms (Townsley et al., in preparation). Chandra studies of 30 Dor have found diffuse, hot gas filling the five H α shells of the region, producing a total X-ray luminosity of $L_X = 4.5 \times 10^{36}$ erg s $^{-1}$ from the diffuse emission in the 0.2–2.0 keV band (Townsley et al. 2006; Lopez et al. 2011).

This paper is structured as follows. In Section 2, we describe the new Chandra observations of H72.97–69.39 and discuss the analysis to produce the X-ray images and spectra. In Section 3, we present the results, including the spatial extent, the nature, and the association of the X-ray emission with YSOs and anti-coincidence with the dense gas. In Section 4.1, we interpret the results in the context of wind bubble models, and in Section 4.2, we compare the X-ray emission of H72.97–69.39 to other Milky Way and LMC sources (by comparison, most SMC HII regions are not X-ray detected; Lopez et al. 2014). We conclude in Section 5.

2. DATA ANALYSIS

2.1. Imaging

H72.97–69.39 in N79-South was observed three times with Chandra ACIS-I in July 2021 for a total of 98 ks (ObsIDs 22473 [29 ks], 23062 [39 ks], and 25091 [30 ks]). Data were reprocessed and reduced using Chandra Interactive Analysis of Observations CIAO version 4.15 (Fruscione et al. 2006). We used the *merge_obs* function

to produce exposure-corrected images (images that are normalized by the effective area across the detectors) in the soft (0.5–1.2 keV), medium (1.2–2.0 keV), hard (2.0–7.0 keV), and broad (0.5–7.0 keV) energy bands (see Figure 2). We detect 209 net broad-band counts within a 1’ radius of H72.97–69.39 in the merged, broad-band image.

2.2. Spectroscopy

In addition to the imaging analysis, we conduct a spectral analysis of the X-rays from H72.97–69.39. Using the CIAO command *specextract*, we extracted spectra from a source region with an area of 1’ \times 1’. The background was extracted from a circular region with a radius of 0.5’ and is $\approx 6.35'$ Southeast of the center of the source region.

We jointly fit the spectra using either thermal or non-thermal plasma models in XSPEC version 12.13.0c (Arnaud 1996). The best fit parameters for these models can be seen in Table 1. The thermal plasma model included a multiplicative constant (CONST), two absorption components (PHABS*PHABS), and one additive thermal plasma component (APEC). The CONST component was allowed to vary to account for the slight variations in flux between the three observations. The first PHABS component was fixed to account for the column density of the Milky Way (MW) in the direction of N79, $N_H^{\text{MW}} = 3.24 \times 10^{21}$ cm $^{-2}$ (HI4PI Collaboration et al. 2016). The second PHABS component, representing the column density of the LMC toward H72.97–69.39, was fixed to $N_H^{\text{LMC}} = 5.5 \times 10^{21}$ cm $^{-2}$ (this value was the upper-limit defined by the XSPEC ERROR command when N_H^{LMC} was allowed to vary). The APEC component, reflecting an optically thin thermal plasma, is defined by its temperature kT , metal abundances, redshift, and a normalization factor. Solar abundances were adopted from Asplund et al. (2009) and set to 0.5 solar metallicity to match the values of the LMC ISM (Kurt & Dufour 1998; Maggi et al. 2016). The temperature and normalization were allowed to vary in the fits.

For comparison, we also tried fitting the data with a power-law component (POWERLAW) representing non-thermal emission in the place of the APEC component. Given the low signal (209 net broad-band counts), we did not attempt a spectral model that included both thermal and non-thermal components as it would be under-constraining (i.e., too many free parameters for the limited degrees of freedom).

3. RESULTS

Figure 2 shows the exposure-corrected, three-color X-ray image of the soft (0.5 – 1.2 keV), medium (1.2 – 2.0 keV), and hard (2.0 – 7.0 keV) X-ray bands around H72.97–69.39. The X-rays are spatially extended $\sim 10'' \approx 2.4$ pc in radius, much greater than the $\approx 0.5''$ on-axis

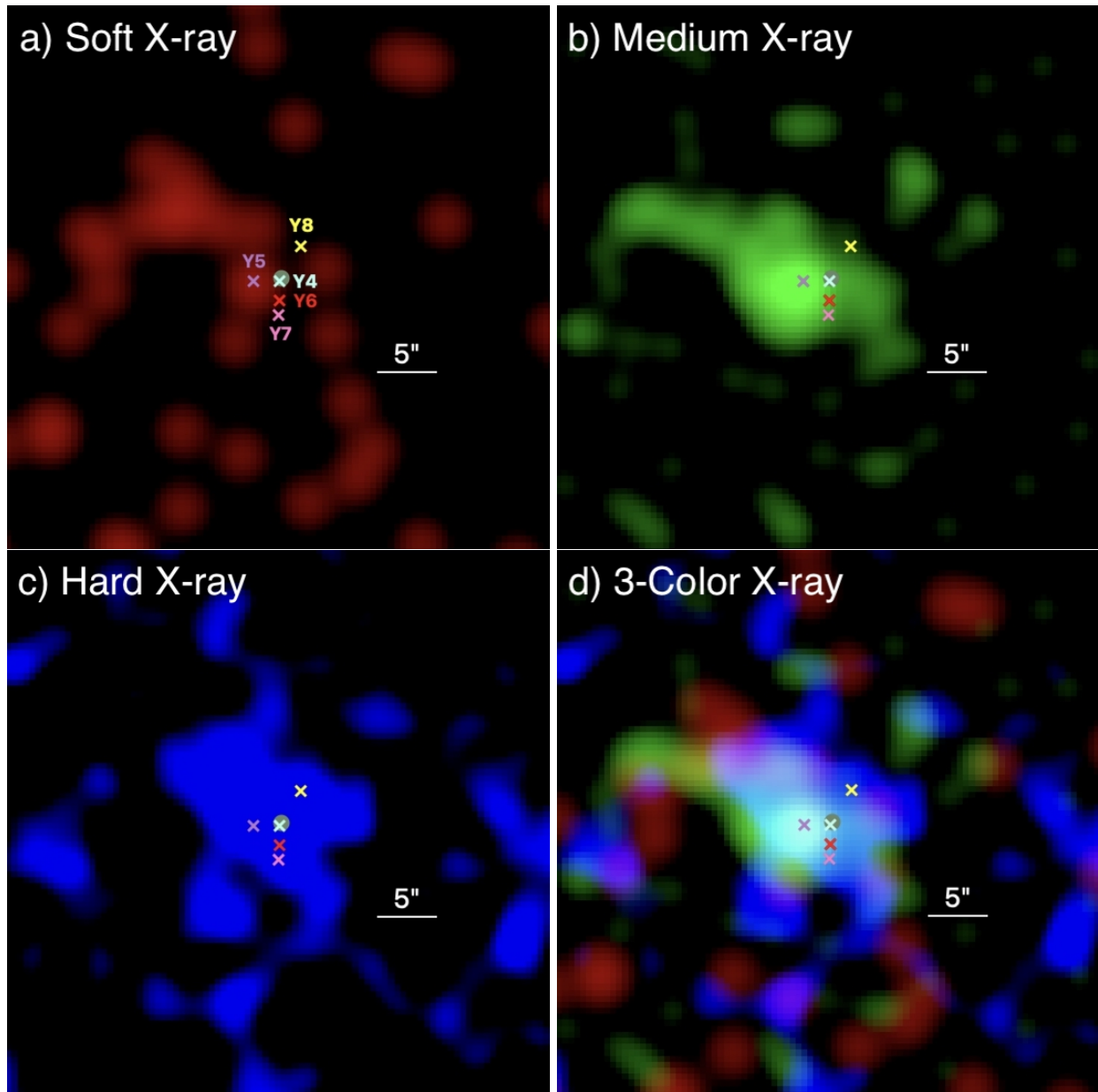


Figure 2. X-ray images of H72.97–69.39 in soft [0.5 – 1.2 keV] (a), medium [1.2 – 2.0 keV] (b), hard [2.0 – 7.0 keV] (c), and all bands (d). The scale bar is $5'' \approx 1.2$ pc, and the images are $0.75' \times 0.75'$ in size. A gray circle marks the position of H72.97–69.39, and five YSO clusters identified by Nayak et al. (2023) with JWST MRS data are labeled with X symbols. North is up, East is left. The X-ray emission is extended $\approx 10''$ and peaks $\approx 5''$ offset from the position of H72.97–69.39.

point spread function (PSF) of Chandra ACIS². The peak of the X-rays is spatially offset $\approx 5'' \approx 1.2$ pc east of the star cluster. It is possible that some emission arises from unresolved point sources coincident with the diffusion emission, but no resolved point sources are apparent in the vicinity of H72.97–69.39.

The X-rays (particularly the medium and hard bands) are spatially coincident with five young stellar object

(YSO) clusters (identified as Y4, Y5, Y6, Y7, and Y8) identified with recent JWST MRS observations (Nayak et al. 2023), as marked in Figure 2. Y4 is coincident with H72.97–69.39, and it is the only one of the five YSO clusters without emission lines associated with polycyclic aromatic hydrocarbons (PAHs) in the MRS spectra, likely stemming from ionizing radiation destroying surrounding PAHs (e.g., Madden et al. 2006; Gordon et al. 2008; Montillaud et al. 2013; Egorov et al. 2023). Y5 is located at the peak of the broad-band X-ray emission and is the only YSO cluster that coincides with soft

² <https://cxc.harvard.edu/proposer/POG/html/chap6.html>.

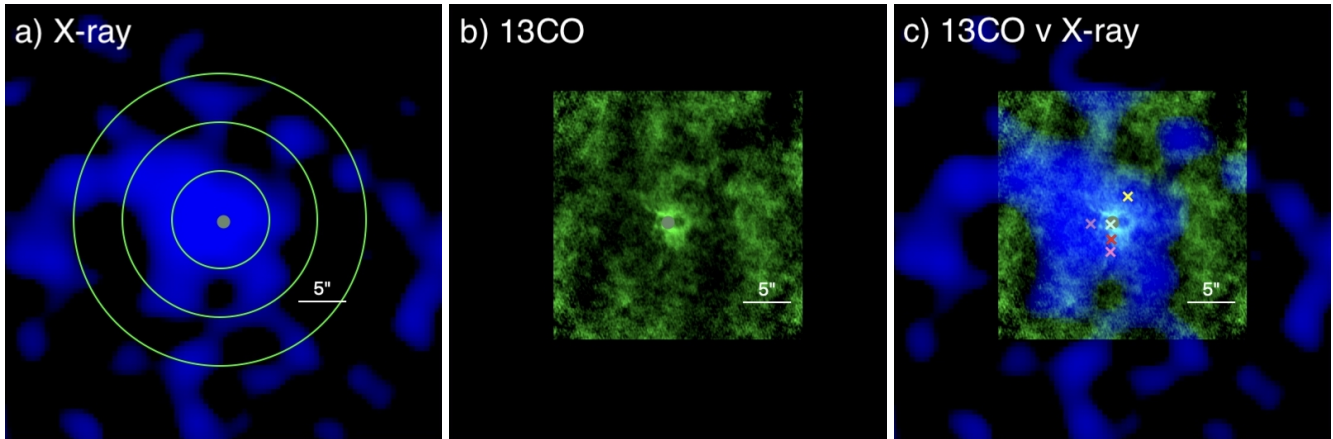


Figure 3. Comparison of the (a) Chandra broad-band (0.5 – 7.0 keV) X-ray emission in blue with the (b) ^{13}CO emission observed with ALMA in green (c) by Nayak et al. (2019). The five YSO clusters identified with JWST by Nayak et al. (2023) are marked with Xs, and H72.97–69.39 is denoted by gray circle in panel (c). The diffuse X-rays appear to fill the low-density cavities where ^{13}CO is dim. Annuli in panel (a) were used to produce the multi-band surface-brightness profiles in Figure 4. All images are $0.75' \times 0.75'$ in size, and the scale bar is $5'' \approx 1.2$ pc at the distance of the LMC.

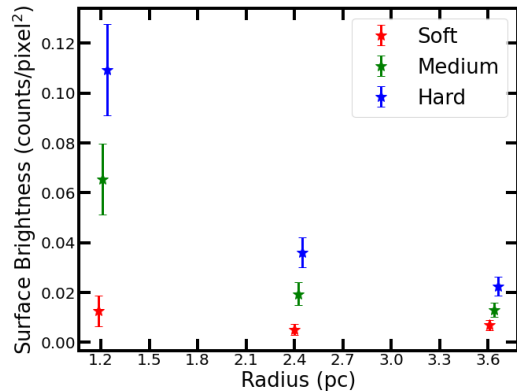


Figure 4. Surface-brightness profile (in units of counts pixel^{-2} of the soft (red), medium (green), and hard (blue) X-ray bands for the three annuli in Figure 3a. The hard X-rays have the greatest surface brightness near H72.97–69.39, and the soft X-rays are the most diffuse/least concentrated relative to the medium and hard X-ray bands.

X-rays. All five YSO clusters have associated hard X-ray emission, and all except Y8 have coincident medium X-ray emission.

To quantify the spatial distribution of the X-ray emission, we measured the surface brightness of the soft, medium, and hard X-ray bands from three annuli centered on H72.97–69.39 with radii of $5''$, $10''$, and $15''$ (see Figure 3a) and produced the profiles plotted in Figure 4. We find that the hard X-rays have the highest surface brightness near H72.97–69.39, while the surface brightness associated with the soft X-ray emission is roughly uniform across the chosen annuli. These profiles suggest that the X-ray emission is hardest around H72.97–69.39 and softens with distance from the star cluster.

X-ray hardness variations across the region may reflect higher column densities $N_{\text{H}}^{\text{LMC}}$ that are absorbing softer X-rays and/or elevated hot gas temperatures kT producing more hard X-rays. Comparison of the broad-band X-ray emission with the ^{13}CO maps of the region from ALMA (Figure 3; Nayak et al. 2019) are consistent with the latter explanation, as the diffuse X-rays appear to fill the low-density cavities where the ^{13}CO is dim.

Although our Chandra program targeted H72.97–69.39, N79S2 (see Figure 1) – another part of N79 South observed with JWST MRS by Nayak et al. (2023) – was also in the field of view. In Figure 5, we show the three-color X-ray image of N79S2. We detect 28 net, broad-band counts that are coincident with the three YSO clusters Y9, Y10, and Y11 identified by Nayak et al. (2023). In particular, the hard X-rays are concentrated to the location of Y11. The angular extent of the emission, $\sim 5''$, is consistent with the off-axis PSF of Chandra, and thus, we are unable to distinguish whether the emission is point-like or diffuse in nature.

The X-ray spectra from H72.97–69.39 (shown in Figure 6) give additional constraints on the emission. Both the single thermal plasma model and the power-law model yield statistically good fits (see Table 1). We find an upper-limit on the LMC column density toward the source of $N_{\text{H}}^{\text{LMC}} = 5.5 \times 10^{21} \text{ cm}^{-2}$, and we fixed it to this value before estimating the other parameters. The thermal plasma model gave a $\chi^2/\text{d.o.f.} = 51/44$ d.o.f. = 1.15 and a best-fit $kT = 3.7_{-1.9}^{+10.0}$ keV. The power-law model produces similar results, with a $\chi^2/\text{d.o.f.} = 49/44 = 1.12$ and a best-fit photon index of $\Gamma = 2.1_{-0.6}^{+0.7}$. The resultant luminosities for the two models are comparable and were $L_{\text{X}} = (1.5 \pm 0.3) \times 10^{34} \text{ erg s}^{-1}$ and $L_{\text{X}} = (1.7 \pm 0.4) \times 10^{34} \text{ erg s}^{-1}$, respectively.

4. DISCUSSION

Table 1. Spectral Model Results

Model	kT (keV)	Γ	$\chi^2/\text{d.o.f.}$	Absorbed Flux ^a (erg cm ⁻² s ⁻¹)	Emitted Flux ^a (erg cm ⁻² s ⁻¹)	Luminosity (erg s ⁻¹)
Thermal Plasma	$3.6^{+10.0}_{-1.9}$	–	51/44	$(3.2 \pm 0.6) \times 10^{-14}$	$(5.1 \pm 1.0) \times 10^{-14}$	$(1.5 \pm 0.3) \times 10^{34}$
Power Law	–	$2.1^{+0.7}_{-0.6}$	49/44	$(3.2 \pm 0.6) \times 10^{-14}$	$(5.8 \pm 1.2) \times 10^{-14}$	$(1.7 \pm 0.4) \times 10^{34}$

^aAbsorbed fluxes are for the 0.5–7.0 keV band adopting a LMC and Milky Way column density of $N_{\text{H}}^{\text{LMC}} = 5.5 \times 10^{21} \text{ cm}^{-2}$ and $N_{\text{H}} = 3.24 \times 10^{21} \text{ cm}^{-2}$, respectively. Emitted fluxes are the unabsorbed fluxes in the same energy bands.

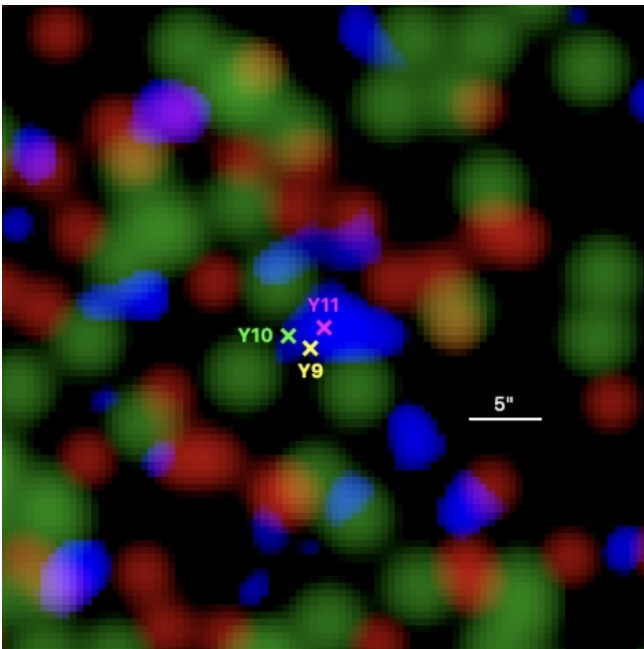


Figure 5. Three-color X-ray image of N79S2, where the soft X-rays (0.5–1.2 keV) are in red, medium X-rays (1.2–2 keV) are in green, and hard X-rays (2–7 keV) are in blue. The three YSO clusters identified with the JWST MRS data from Nayak et al. (2023) are labeled. The hard X-rays dominate this source, likely because of high absorbing column toward it. The image is $0.75' \times 0.75'$; the scale bar is $5'' \approx 1.2 \text{ pc}$ at the distance of the LMC.

In Section 3, we found that H72.97–69.39 (and the associated YSO clusters identified with JWST) has coincident diffuse X-ray emission. The flux in the medium and hard bands is more centrally concentrated than the soft X-rays, and the X-ray spectrum can be modeled as a thermal plasma or with a power-law. In Section 4.1, we compare these results to predictions from wind models, and in Section 4.2, we discuss how the X-ray properties of H72.97–69.39 compare to those of other young MSCs in the Milky Way and LMC.

4.1. Comparison to Wind Models X-ray Predictions

In an idealized HII region powered by a MSC, wind energy is injected at a rate of

$$L_w = \sum_{i=1}^N \frac{1}{2} \dot{M}_{w,i} v_{w,i}^2, \quad (1)$$

where $\dot{M}_{w,i}$ and $v_{w,i}$ are the mass-loss rate and wind velocity for individual stars i that are summed over the total N stars in the cluster. Typical values of L_w for Milky Way and LMC MSCs are $L_w \sim 10^{37} - 10^{39} \text{ erg s}^{-1}$ (e.g., Smith 2006; Rosen et al. 2014). We can estimate L_w for H72.97–69.39 assuming $L_{\text{bol}} = 2.2 \times 10^6 L_{\odot}$ (Ochsendorf et al. 2017) and relating it to the expected total wind luminosity using stellar population synthesis and a prescription for wind mass loss and velocity.

In particular, we first download isochrones of $[\text{Fe}/\text{H}] = -0.25$ (meant to approximate $Z = 0.5Z_{\odot}$, the LMC ISM metallicity: Kurt & Dufour 1998; Maggi et al. 2016) from the MIST³ database (Choi et al. 2016; Dotter 2016). We then generate a large (total mass $10^6 M_{\odot}$) sample of masses following the Kroupa IMF (Kroupa 2001) with minimum and maximum masses of $M_{\text{min}} = 0.01 M_{\odot}$ and $M_{\text{max}} = 200 M_{\odot}$. We use the MIST isochrones to derive bolometric luminosities for each star in the sample as a function of time. Assuming the mass-loss rates of Vink et al. (2000, 2001), we also calculate the wind mass loss and wind velocities of all stars with mass $M_* > 8 M_{\odot}$ in the sample and use Equation 1 to calculate their wind luminosities.

At each point in time (time-steps determined by the age steps of the MIST isochrones), we sum the bolometric and mechanical wind luminosities over all stars in the sample and divide by the total mass of the sample to arrive at population-averaged values for L_{bol}/M_* and L_w/M_* . We average these ratios over ages $< 2 \text{ Myr}$, roughly the period over which wind luminosities remain roughly constant before the onset of SNe (Lancaster et al. 2021a). We obtain $L_{\text{bol}}/M_* = 1.37 \times 10^3 L_{\odot}/M_{\odot}$ and $L_w/M_* = 4.20 L_{\odot}/M_{\odot}$. Given the L_{bol}

³ <https://waps.cfa.harvard.edu/MIST/>

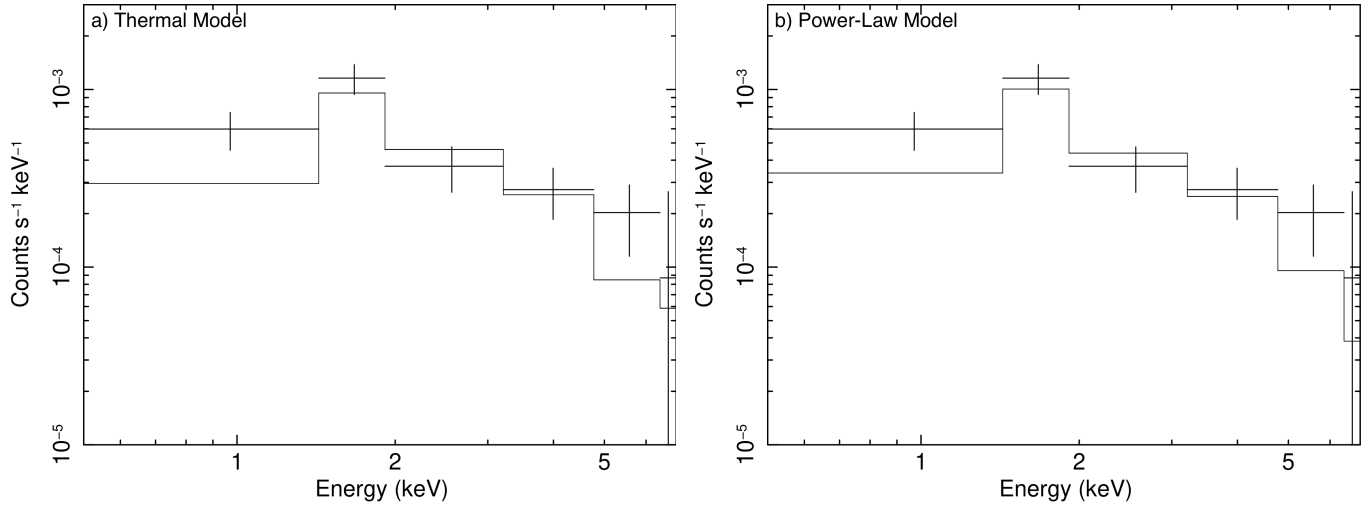


Figure 6. Extracted, background-subtracted spectra from a $1' \times 1'$ region around H72.97–69.39 with the best-fit thermal plasma model (a) and power-law model (b) overplotted. The best-fit parameters are listed in Table 1. Both models produce statistically good fits and predict similar X-ray luminosities from the source.

of H72.97–69.39, we estimate a mechanical wind luminosity of $L_w = 6.7 \times 10^3 L_\odot = 2.6 \times 10^{37} \text{ erg s}^{-1}$.

In order to relate this value to an expected X-ray luminosity L_X in the bubble, we need to consult a model for wind-blown bubble evolution. The theoretical models of Castor et al. (1975) and Weaver et al. (1977) predict X-ray luminosities assuming the shock-heated gas is confined by a cool shell of swept-up ISM. Additionally, this cool shell is heated by the bubble’s hot gas through thermal conduction, resulting in evaporation and mass loading of the bubble interior, resulting in higher X-ray luminosities. An alternative model by Chevalier & Clegg (1985) ignores the surrounding ISM and assumes a steady, freely-expanding wind, equivalent to assuming that the “free-wind” of the Weaver et al. (1977) model occupies the entire bubble volume. As the Castor and Weaver models can over-predict X-ray luminosity and Chevalier & Clegg can under-predict it, Harper-Clark & Murray (2009) introduced an intermediate model, where hot gas expands into an inhomogeneous ISM, creating a porous shell from which hot gas can escape/leak. Leakage is one mechanism by which energy can be lost from bubbles producing lower-than-expected X-ray luminosities (e.g., Lopez et al. 2011; Rosen et al. 2014). Other mechanisms have been proposed as possible sinks for the wind energy, chiefly turbulent mixing with the surrounding gas followed by radiative cooling (Rosen et al. 2014; Lancaster et al. 2021b; Rosen 2022).

The differences between these wind energy loss channels are likely dependent on the detailed density and temperature structure in the bubble’s interior, particularly at its interface. Here we simply present the predictions for X-ray luminosity L_X and radius R assuming a single density and temperature as predicted for a Weaver et al. (1977) model. The Weaver et al. model requires an assumption of the background number

density of the surrounding cloud; measurements from Ochsendorf et al. (2017) indicate a molecular gas mass $M_{\text{gas,H}_2} \approx 10^5 M_\odot$ within $R = 10^{1.4} \text{ pc} \approx 25 \text{ pc}$ (see their Figure 5). In the same region atomic gas contributes about one-third as much mass and ionized gas contributes negligibly, indicating an average gas density of $\rho \approx 2 M_\odot \text{ pc}^{-3} = 1.4 \times 10^{-22} \text{ g cm}^{-3}$.

Assuming an X-ray extent of $10'' \approx 2.4 \text{ pc}$ (Section 3) is the radius of the wind bubble R_b , we can use the Weaver et al. (1977) model to estimate the bubble age t , the predicted temperature T_b , and the X-ray luminosity L_X . From Equation 21 of Weaver et al. (1977),

$$t = \left(\frac{125}{154\pi} \right)^{-1/3} L_w^{-1/3} \rho^{1/3} R_b^{5/3} \quad (2)$$

which yields $t = 2.4 \times 10^4 \text{ yr}$. This age is younger than the estimated age of the YSO clusters; e.g. the molecular gas outflows from H72.97–69.39 have an associated timescale of $\approx 6.5 \times 10^4 \text{ yr}$ (Nayak et al. 2019). From t , the Weaver model predicts a bubble temperature T_b of (their Equation 37)

$$T_b = 2.07 \times 10^6 L_{36}^{8/35} n_0^{2/35} t_6^{-6/35} \text{ K}, \quad (3)$$

where $L_{36} \equiv L_w/10^{36} \text{ erg s}^{-1}$, $t_6 \equiv t/10^6 \text{ yr}$, and $n_0 = \rho/\mu m_p$ is the ambient number density. Assuming a mean molecular weight of $\mu = 1.4$ for the background gas, we find $T_b = 1.0 \times 10^7 \text{ K}$, corresponding to $kT = 0.9 \text{ keV}$. This value is statistically lower than our estimated $kT = 3.6_{-1.9}^{+10.0} \text{ keV}$ from X-ray spectral modeling (see Table 1). As the Weaver et al. (1977) model does not take into account cooling at the bubble-shell interface, it over-estimates the mass-loading of the bubble interior, leading to an under-estimate of T_b (see e.g. Eq. 45 of El-Badry et al. 2019), consistent with what we see here.

Table 2. Characteristics of Star-Forming Regions with Detected Diffuse X-ray Emission

Region	Age (Myr)	Distance (kpc)	L_{bol} (L_{\odot})	L_X (erg s^{-1})	References
RCW 38	0.1–0.5	1.7	9.7×10^5	1.5×10^{33}	1, 2, 3
N79	0.5	50	7.8×10^7	1.5×10^{34}	this work
NGC 3603 ^a	1	7.0	2.3×10^7	2.6×10^{35}	4, 5, 6
Arches Cluster ^b	1–2	8.5	...	1.6×10^{34}	7
30 Doradus ^a	1–2	50	7.8×10^7	4.5×10^{36}	8
Carina Nebula	2–3	2.3	2.5×10^7	1.7×10^{35}	6
Rosette Nebula	2–4	1.4	2.3×10^6	6.0×10^{32}	9, 10, 11
Westerlund 1	3–4	5.0	2.6×10^6	3.0×10^{34}	5, 12

^a L_X corresponding to the soft-band (0.5–2.0 keV) diffuse emission.

^bDue to extinction uncertainties toward the Galactic Center, this L_{bol} has substantial uncertainty (Clark et al. 2018).

References—(1) Wolk et al. (2006); (2) Fukui et al. (2016); (3) Pandey et al. (2024); (4) Moffat et al. (2002); (5) Binder & Povich (2018); (6) Townsley et al. (2011); (7) Yusef-Zadeh et al. (2002); (8) Lopez et al. (2011); (9) Bruhweiler et al. (2010); (10) Cox et al. (1990); (11) Townsley et al. (2003); (12) Munro et al. (2006)

Finally, we combine the above derived quantities with X-ray emissivities calculated with `yt`'s X-ray emissivity calculator (Turk et al. 2011) to find an associated X-ray luminosity in the 0.5–7 keV band for the Weaver et al. (1977) model of $L_X = 3.4 \times 10^{35} \text{ erg s}^{-1}$. This value is about an order of magnitude larger than the observed L_X (see Table 1). We can get another estimate of the X-ray luminosity from the Weaver et al. (1977) model by following the derivation of Appendix B of Chu & Mac Low (1990), which takes into account the temperature and density variation in the bubble's interior due to the evaporative mass flow in the Weaver et al. (1977) model. Using their Equation B7 we infer an X-ray luminosity of $L_X = 1.0 \times 10^{35} \text{ erg s}^{-1}$, which is still an order of magnitude larger than the observed value.

These estimates, combined with the very young age inferred from the application of the Weaver et al. (1977) model through Equation 2, indicates that there is likely significant cooling at the wind bubble's interface. Such cooling would both reduce the efficiency of the bubble's expansion (Rosen et al. 2014; Lancaster et al. 2021a,b), explaining an older age, and reduce the mass-loading of the bubble from conductive evaporation (El-Badry et al. 2019), explaining a lower L_X . Numerical simulations following the formation of individual massive stars have confirmed that these effects occur early (Rosen 2022).

4.2. Comparison to Other Young Star Clusters

Diffuse X-ray emission associated with gas shock-heated by stellar wind feedback has been detected in many other young star-forming regions, including NGC 3603 (Moffat et al. 2002), the Arches Cluster

(Yusef-Zadeh et al. 2002), RCW 38 (Wolk et al. 2002; Fukushima et al. 2023), M17 (Townsley et al. 2003), the Rosette Nebula (Townsley et al. 2003), Westerlund 1 (Munro et al. 2006), the Carina Nebula (Townsley et al. 2011), and 30 Doradus (Townsley et al. 2006; Lopez et al. 2011). The characteristics of these star-forming regions are shown in Table 2, spanning two orders of magnitude in bolometric luminosity L_{bol} and four orders of magnitude in L_X .

One region with a young age similar to H72.97–69.39 is the Milky Way HII region RCW 38 which is estimated to be 0.1–0.5 Myr old (Wolk et al. 2006; Fukui et al. 2016). RCW 38 has ~ 80 times lower bolometric luminosity (with $L_{\text{bol}} = 9.7 \times 10^5 L_{\odot}$), an order of magnitude lower X-ray luminosity (with $L_X = (1.5 \pm 0.2) \times 10^{33} \text{ erg s}^{-1}$), and a slightly higher hot gas temperature (with $kT = 4.5_{-0.9}^{+1.2} \text{ keV}$) than H72.97–69.39 (Pandey et al. 2024). The diffuse X-ray emission of RCW 38 requires both thermal and non-thermal components to fit the spectra (Wolk et al. 2002; Fukushima et al. 2023; Pandey et al. 2024), whereas the weaker signal from H72.97–69.39 does not enable us to distinguish whether both components are necessary to model the data adequately. Both H72.97–69.39 and RCW 38 demonstrate that diffuse X-rays associated with stellar winds are produced early in MSC formation.

5. CONCLUSIONS

In this work, we present new Chandra observations totaling 98 ks toward the potential superstar cluster (SSC) H72.97–69.39 in N79-South. We detect ~ 200 net, broad-band X-ray counts from the 1' vicinity of

H72.97–69.39 where five YSO clusters have been identified using JWST (see Figure 2). We also serendipitously detect ~ 30 net counts from another location in N79-South with three YSO clusters (see Figure 5). The X-ray emission is extended $\sim 10''$ in radius, much greater than the Chandra on-axis PSF, demonstrates that diffuse hot gas is produced by stellar-wind feedback in the earliest stages of formation.

We show that the X-ray emission around H72.97–69.39 is especially hard, dominated by photons above 1.2 keV, suggesting a high hot gas temperature, a large absorbing column in the region, and/or contribution from a non-thermal/power-law component. The X-rays appear to be spatially anti-coincident with the ^{13}CO dense gas (Figure 3), suggesting that the hot gas is preferentially occupying the lower-density cavities.

Comparison to stellar wind model predictions shows that the X-ray luminosity of H72.97–69.39 is about one order of magnitude below expected if the shock-heated gas is confined by a cool shell that heats up via thermal conduction and evaporates. This result suggests that, even this early in the MSC formation process, significant amounts of wind energy are being lost. Likely ex-

planations are either turbulent mixing followed by radiative cooling (Rosen et al. 2014; Lancaster et al. 2021a,b) or physical leakage of the gas (Harper-Clark & Murray 2009), with the former likely playing a larger role (Lancaster et al. 2021c).

Software: CIAO (v4.15; Fruscione et al. 2006), XSPEC (v12.13.0c; Arnaud 1996)

ACKNOWLEDGMENTS

Support for this work was provided by the National Aeronautics and Space Administration through Chandra Award Number GO0-21071X issued by the Chandra X-ray Center, which is operated by the Smithsonian Astrophysical Observatory for and on behalf of the National Aeronautics Space Administration under contract NAS8-03060. JR and LAL also acknowledge support through the Heising-Simons Foundation grant 2022-3533. LAL and LL gratefully acknowledges the support of the Simons Foundation.

REFERENCES

- Agertz, O., Kravtsov, A. V., Leitner, S. N., & Gnedin, N. Y. 2013, *ApJ*, 770, 25, doi: [10.1088/0004-637X/770/1/25](https://doi.org/10.1088/0004-637X/770/1/25)
- Arnaud, K. A. 1996, in *Astronomical Society of the Pacific Conference Series*, Vol. 101, *Astronomical Data Analysis Software and Systems V*, ed. G. H. Jacoby & J. Barnes, 17
- Asplund, M., Grevesse, N., Sauval, A. J., & Scott, P. 2009, *ARA&A*, 47, 481, doi: [10.1146/annurev.astro.46.060407.145222](https://doi.org/10.1146/annurev.astro.46.060407.145222)
- Binder, B. A., & Povich, M. S. 2018, *ApJ*, 864, 136, doi: [10.3847/1538-4357/aad7b2](https://doi.org/10.3847/1538-4357/aad7b2)
- Bruhweiler, F. C., Freire Ferrero, R., Bourdin, M. O., & Gull, T. R. 2010, *ApJ*, 719, 1872, doi: [10.1088/0004-637X/719/2/1872](https://doi.org/10.1088/0004-637X/719/2/1872)
- Cantó, J., Raga, A. C., & Rodríguez, L. F. 2000, *ApJ*, 536, 896, doi: [10.1086/308983](https://doi.org/10.1086/308983)
- Castor, J., McCray, R., & Weaver, R. 1975, *ApJL*, 200, L107, doi: [10.1086/181908](https://doi.org/10.1086/181908)
- Chevalier, R. A., & Clegg, A. W. 1985, *Nature*, 317, 44, doi: [10.1038/317044a0](https://doi.org/10.1038/317044a0)
- Choi, J., Dotter, A., Conroy, C., et al. 2016, *ApJ*, 823, 102, doi: [10.3847/0004-637X/823/2/102](https://doi.org/10.3847/0004-637X/823/2/102)
- Chu, Y.-H., & Mac Low, M.-M. 1990, *ApJ*, 365, 510, doi: [10.1086/169505](https://doi.org/10.1086/169505)
- Clark, J. S., Lohr, M. E., Najarro, F., Dong, H., & Martins, F. 2018, *A&A*, 617, A65, doi: [10.1051/0004-6361/201832826](https://doi.org/10.1051/0004-6361/201832826)
- Cox, P., Deharveng, L., & Leene, A. 1990, *A&A*, 230, 181
- Dotter, A. 2016, *ApJS*, 222, 8, doi: [10.3847/0067-0049/222/1/8](https://doi.org/10.3847/0067-0049/222/1/8)
- Egorov, O. V., Kreckel, K., Sandstrom, K. M., et al. 2023, *ApJL*, 944, L16, doi: [10.3847/2041-8213/acac92](https://doi.org/10.3847/2041-8213/acac92)
- El-Badry, K., Ostriker, E. C., Kim, C.-G., Quataert, E., & Weisz, D. R. 2019, *MNRAS*, 490, 1961, doi: [10.1093/mnras/stz2773](https://doi.org/10.1093/mnras/stz2773)
- Fruscione, A., McDowell, J. C., Allen, G. E., et al. 2006, in *Society of Photo-Optical Instrumentation Engineers (SPIE) Conference Series*, Vol. 6270, *Society of Photo-Optical Instrumentation Engineers (SPIE) Conference Series*, ed. D. R. Silva & R. E. Doxsey, 62701V, doi: [10.1117/12.671760](https://doi.org/10.1117/12.671760)
- Fukui, Y., Torii, K., Ohama, A., et al. 2016, *ApJ*, 820, 26, doi: [10.3847/0004-637X/820/1/26](https://doi.org/10.3847/0004-637X/820/1/26)
- Fukushima, A., Ezoe, Y., & Odaka, H. 2023, *PASJ*, 75, 187, doi: [10.1093/pasj/psac100](https://doi.org/10.1093/pasj/psac100)
- Gordon, K. D., Engelbracht, C. W., Rieke, G. H., et al. 2008, *ApJ*, 682, 336, doi: [10.1086/589567](https://doi.org/10.1086/589567)
- Harper-Clark, E., & Murray, N. 2009, *ApJ*, 693, 1696, doi: [10.1088/0004-637X/693/2/1696](https://doi.org/10.1088/0004-637X/693/2/1696)
- HI4PI Collaboration, Ben Bekhti, N., Flöer, L., et al. 2016, *A&A*, 594, A116, doi: [10.1051/0004-6361/201629178](https://doi.org/10.1051/0004-6361/201629178)
- Hunter, D. A., Shaya, E. J., Holtzman, J. A., et al. 1995, *ApJ*, 448, 179, doi: [10.1086/175950](https://doi.org/10.1086/175950)

- Kroupa, P. 2001, *MNRAS*, 322, 231,
doi: [10.1046/j.1365-8711.2001.04022.x](https://doi.org/10.1046/j.1365-8711.2001.04022.x)
- Krumholz, M. R., McKee, C. F., & Bland-Hawthorn, J. 2019, *ARA&A*, 57, 227,
doi: [10.1146/annurev-astro-091918-104430](https://doi.org/10.1146/annurev-astro-091918-104430)
- Kurt, C. M., & Dufour, R. J. 1998, in *Revista Mexicana de Astronomia y Astrofisica Conference Series*, Vol. 7, *Revista Mexicana de Astronomia y Astrofisica Conference Series*, ed. R. J. Dufour & S. Torres-Peimbert, 202
- Lancaster, L., Ostriker, E. C., Kim, J.-G., & Kim, C.-G. 2021a, *ApJ*, 914, 89, doi: [10.3847/1538-4357/abf8ab](https://doi.org/10.3847/1538-4357/abf8ab)
- . 2021b, *ApJ*, 914, 90, doi: [10.3847/1538-4357/abf8ac](https://doi.org/10.3847/1538-4357/abf8ac)
- . 2021c, *ApJL*, 922, L3, doi: [10.3847/2041-8213/ac3333](https://doi.org/10.3847/2041-8213/ac3333)
- Lopez, L. A., Krumholz, M. R., Bolatto, A. D., Prochaska, J. X., & Ramirez-Ruiz, E. 2011, *ApJ*, 731, 91,
doi: [10.1088/0004-637X/731/2/91](https://doi.org/10.1088/0004-637X/731/2/91)
- Lopez, L. A., Krumholz, M. R., Bolatto, A. D., et al. 2014, *ApJ*, 795, 121, doi: [10.1088/0004-637X/795/2/121](https://doi.org/10.1088/0004-637X/795/2/121)
- Madden, S. C., Galliano, F., Jones, A. P., & Sauvage, M. 2006, *A&A*, 446, 877, doi: [10.1051/0004-6361:20053890](https://doi.org/10.1051/0004-6361:20053890)
- Maggi, P., Haberl, F., Kavanagh, P. J., et al. 2016, *A&A*, 585, A162, doi: [10.1051/0004-6361/201526932](https://doi.org/10.1051/0004-6361/201526932)
- Malumuth, E. M., & Heap, S. R. 1994, *AJ*, 107, 1054,
doi: [10.1086/116917](https://doi.org/10.1086/116917)
- Meixner, M., Gordon, K. D., Indebetouw, R., et al. 2006, *AJ*, 132, 2268, doi: [10.1086/508185](https://doi.org/10.1086/508185)
- Moffat, A. F. J., Corcoran, M. F., Stevens, I. R., et al. 2002, *ApJ*, 573, 191, doi: [10.1086/340491](https://doi.org/10.1086/340491)
- Montillaud, J., Joblin, C., & Toubanc, D. 2013, *A&A*, 552, A15, doi: [10.1051/0004-6361/201220757](https://doi.org/10.1051/0004-6361/201220757)
- Muno, M. P., Law, C., Clark, J. S., et al. 2006, *ApJ*, 650, 203, doi: [10.1086/507175](https://doi.org/10.1086/507175)
- Nayak, O., Meixner, M., Sewilo, M., et al. 2019, *ApJ*, 877, 135, doi: [10.3847/1538-4357/ab1b38](https://doi.org/10.3847/1538-4357/ab1b38)
- Nayak, O., Hirschauer, A., Kavanagh, P., et al. 2023, submitted to *ApJ*
- Ochsendorf, B. B., Zinnecker, H., Nayak, O., et al. 2017, *Nature Astronomy*, 1, 784,
doi: [10.1038/s41550-017-0268-0](https://doi.org/10.1038/s41550-017-0268-0)
- Pandey, P., Lopez, L. A., Rosen, A. L., et al. 2024, submitted to *ApJ*
- Rosen, A. L. 2022, *ApJ*, 941, 202,
doi: [10.3847/1538-4357/ac9f3d](https://doi.org/10.3847/1538-4357/ac9f3d)
- Rosen, A. L., Lopez, L. A., Krumholz, M. R., & Ramirez-Ruiz, E. 2014, *MNRAS*, 442, 2701,
doi: [10.1093/mnras/stu1037](https://doi.org/10.1093/mnras/stu1037)
- Seale, J. P., Meixner, M., Sewilo, M., et al. 2014, *AJ*, 148, 124, doi: [10.1088/0004-6256/148/6/124](https://doi.org/10.1088/0004-6256/148/6/124)
- Smith, N. 2006, *MNRAS*, 367, 763,
doi: [10.1111/j.1365-2966.2006.10007.x](https://doi.org/10.1111/j.1365-2966.2006.10007.x)
- Smith, R. C., & MCELS Team. 1998, *PASA*, 15, 163,
doi: [10.1071/AS98163](https://doi.org/10.1071/AS98163)
- Stevens, I. R., & Hartwell, J. M. 2003, *MNRAS*, 339, 280,
doi: [10.1046/j.1365-8711.2003.06184.x](https://doi.org/10.1046/j.1365-8711.2003.06184.x)
- Townsley, L. K., Broos, P. S., Chu, Y.-H., et al. 2011, *ApJS*, 194, 16, doi: [10.1088/0067-0049/194/1/16](https://doi.org/10.1088/0067-0049/194/1/16)
- Townsley, L. K., Broos, P. S., Feigelson, E. D., et al. 2006, *AJ*, 131, 2140, doi: [10.1086/500532](https://doi.org/10.1086/500532)
- Townsley, L. K., Feigelson, E. D., Montmerle, T., et al. 2003, *ApJ*, 593, 874, doi: [10.1086/376692](https://doi.org/10.1086/376692)
- Turk, M. J., Smith, B. D., Oishi, J. S., et al. 2011, *The Astrophysical Journal Supplement Series*, 192, 9,
doi: [10.1088/0067-0049/192/1/9](https://doi.org/10.1088/0067-0049/192/1/9)
- Vink, J. S., de Koter, A., & Lamers, H. J. G. L. M. 2000, *A&A*, 362, 295, doi: [10.48550/arXiv.astro-ph/0008183](https://doi.org/10.48550/arXiv.astro-ph/0008183)
- . 2001, *A&A*, 369, 574, doi: [10.1051/0004-6361:20010127](https://doi.org/10.1051/0004-6361:20010127)
- Weaver, R., McCray, R., Castor, J., Shapiro, P., & Moore, R. 1977, *ApJ*, 218, 377, doi: [10.1086/155692](https://doi.org/10.1086/155692)
- Wolk, S. J., Bourke, T. L., Smith, R. K., Spitzbart, B., & Alves, J. 2002, *ApJL*, 580, L161, doi: [10.1086/345611](https://doi.org/10.1086/345611)
- Wolk, S. J., Spitzbart, B. D., Bourke, T. L., & Alves, J. 2006, *AJ*, 132, 1100, doi: [10.1086/505704](https://doi.org/10.1086/505704)
- Wong, T., Hughes, A., Ott, J., et al. 2011, *ApJS*, 197, 16,
doi: [10.1088/0067-0049/197/2/16](https://doi.org/10.1088/0067-0049/197/2/16)
- Yusef-Zadeh, F., Law, C., Wardle, M., et al. 2002, *ApJ*, 570, 665, doi: [10.1086/340058](https://doi.org/10.1086/340058)